

ENERGY MINIMIZATION IN TWO-LEVEL DISSIPATIVE QUANTUM CONTROL: THE INTEGRABLE CASE

BERNARD BONNARD, JEAN-BAPTISTE CAILLAU AND OLIVIER COTS

Math. Institute, Bourgogne Univ. & CNRS
9 avenue Savary, F-21078 Dijon, France

ABSTRACT. The aim of this contribution is to refine some of the computations of [6]. The Lindblad equation modelling a two-level dissipative quantum system is investigated. The control can be interpreted as the action of a laser to rotate a molecule in gas phase, or as the effect of a magnetic field on a spin 1/2 particle. For the energy cost, normal extremals of the maximum principle are solution to a three-dimensional Hamiltonian with parameters. The analysis is focussed on an integrable submodel which defines outside singularities a pseudo-Riemannian metric in dimension five. Complete quadratures are given for this subcase by means of Weierstraß elliptic functions. Preliminary computations of cut and conjugate loci are also provided for a two-dimensional restriction using [9].

Introduction. We are concerned with the bilinear Lindblad equations describing the dynamics of a two-level dissipative quantum system,

$$\dot{x}_1 = -\Gamma x_1 + u_2 x_3, \quad (1)$$

$$\dot{x}_2 = -\Gamma x_2 - u_1 x_3, \quad (2)$$

$$\dot{x}_3 = \tilde{\gamma} - \gamma x_3 + u_1 x_2 - u_2 x_1, \quad (3)$$

where $2\Gamma \geq \gamma \geq |\tilde{\gamma}|$ are dissipation parameters modelling the interaction with the environment (*e.g.*, molecular collisions). The state $x \in \mathbf{R}^3$ represents in suitable coordinates the density matrix of the quantum system. The control $u = (u_1, u_2) \in \mathbf{R}^2$ can be an electric or a magnetic field.

The recent interest in such problems comes from several applications. Among them, we can mention molecular alignment in gas phase using a laser field, and control of the dynamics of spin 1/2 particles in liquid phase using nuclear magnetic resonance. The conservative case (that is without dissipation) has been addressed in several papers (see, *e.g.*, [7, 10]). We focus here on the more complex dissipative situation. While final time minimization is studied in [5], we consider the so-called energy criterion,

$$\int_0^{t_f} (u_1^2 + u_2^2) dt \rightarrow \min,$$

2000 *Mathematics Subject Classification.* Primary: 49K15, 81Q05.

Key words and phrases. Optimal control, Lindblad equation, Lorentzian metrics, elliptic functions, conjugate and cut loci.

The first and second authors are supported by ANR Geometric Control Methods (project no. NT09_504490). The second author is supported by SADCO Initial Training Network (FP7 grant no. 264735-SADCO). The second and third authors are supported by Conseil Régional de Bourgogne (contract no. 2009-160E-160-CE-160T).

without any bound on the control. Existence results for this problem are given in [6], as well as preliminary computations of optimal trajectories in a particular integrable subcase of the model. We propose here a straightforward algebraic derivation of the latter. This will lay the emphasis on the classification of optimal curves by a single integer, the genus of the complex algebraic curve behind the computations. It will also provide quadratures well suited for further studies, in particular estimates of cut and conjugate points in relation with global and local optimality of trajectories.

In the first section, we recall Pontryagin maximum principle and reduce the study to an integrable Hamiltonian submodel (with parameters) on the two-sphere. Quadratures of the resulting extremal flow are given in section 2. The last section is devoted to a preliminary analysis of cut and conjugate loci of the submodel.

1. Normal extremals. According to Pontryagin maximum principle, optimal trajectories are projection on the state space of solutions (*extremals*) in $T^*\mathbf{R}^3$ of the following Hamiltonian,

$$H(x, p) = p^0(u_1^2 + u_2^2) + H_0 + u_1H_1 + u_2H_2.$$

Here, $p^0 \leq 0$ is a parameter, (x, p) are coordinates on the cotangent bundle, and $H_i = \langle p, F(x) \rangle$, $i = 0, 2$, are Hamiltonian lifts of the vector fields defining the dynamics (1-3),

$$\dot{x} = F_0(x) + u_1F_1(x) + u_2F_2(x)$$

with

$$F_0 = -\Gamma(x_1 \frac{\partial}{\partial x_1} + x_2 \frac{\partial}{\partial x_2}) + (\tilde{\gamma} - \gamma x_3) \frac{\partial}{\partial x_3},$$

$$F_1 = -x_3 \frac{\partial}{\partial x_2} + x_2 \frac{\partial}{\partial x_3}, \quad F_2 = x_3 \frac{\partial}{\partial x_1} - x_1 \frac{\partial}{\partial x_3}.$$

Moreover, the Hamiltonian has to be maximized almost everywhere with respect to u along the extremal. It is homogeneous in (p^0, p) and there are two situations: The *normal case* $p^0 \neq 0$, and the *abnormal case* $p^0 = 0$. Restricting to normal extremals (see [6] for the abnormal one) and normalizing p^0 to $-1/2$, the maximization condition leads to $u = (H_1, H_2)$ which allows to express the control as a function of (x, p) . Plugging this function into H defines the *true Hamiltonian* of the problem,

$$H = H_0 + \frac{1}{2}(H_1^2 + H_2^2).$$

We make a change of variables both on the state and on the parameters, passing to suited spherical coordinates

$$(x_1, x_2, x_3) = e^r(\sin \varphi \cos \theta, \sin \varphi \sin \theta, \cos \varphi),$$

and setting $\delta = \Gamma - \gamma$. Then,

$$H_0 = -(\delta \sin^2 \varphi + \gamma)p_r - \delta \cos \varphi \sin \varphi p_\varphi - \tilde{\gamma}e^{-r}(p_r \cos \varphi - p_\varphi \sin \varphi).$$

$$H_1 = -\frac{p_\theta}{\tan \varphi}, \quad H_2 = p_\varphi.$$

Proposition 1. *For $\tilde{\gamma} = 0$, the system is Liouville integrable.*

Proof. As both coordinates r and θ are cyclic, p_r and p_θ define two additional linear first integrals. □

The Hamiltonian is quadratic in $(p_r, p_\theta, p_\varphi, \delta, \gamma, \tilde{\gamma})$, and easily checked to be everywhere degenerate as a form in dimension six. Nevertheless, restricting to the integrable submodel,

$$\begin{aligned} H &= \frac{1}{2} \frac{p_\theta^2}{\tan^2 \varphi} + \frac{1}{2} (p_\varphi - \delta \cos \varphi \sin \varphi)^2 - \frac{1}{2} (\delta \cos \varphi \sin \varphi + p_r \tan \varphi)^2 \\ &+ \frac{1}{2} (p_r \tan \varphi - \frac{\gamma}{\tan \varphi})^2 - \frac{1}{2} \frac{\gamma^2}{\tan^2 \varphi}. \end{aligned}$$

Parameters δ and γ can be interpreted as duals to cyclic variables, and the following holds.

Proposition 2. *The integrable submodel defines a $(3, 2)$ pseudo-Riemannian metric in dimension five with a singularity at $\varphi = \pi/2$. The restriction to $p_r = 0$ is Lorentzian in dimension three outside the singularity.*

Proof. The determinant of the quadratic form in $(p_r, p_\theta, p_\varphi, \delta, \gamma)$ is equal to $\cos^4 \varphi$. \square

2. Integration of the flow. On the level set $H = h$, integrability for $\tilde{\gamma} = 0$ is also clear as the system can be rewritten in the mechanical form

$$\frac{1}{2} \dot{\varphi}^2 + V(\varphi, p_r, p_\theta, \delta, \gamma) = h$$

where the potential is

$$V(\varphi, p_r, p_\theta, \delta, \gamma) = \frac{1}{2} \frac{p_\theta^2}{\tan^2 \varphi} - \frac{\delta^2}{2} \cos^2 \varphi \sin^2 \varphi - (\delta \sin^2 \varphi + \gamma) p_r.$$

Setting $X = \sin^2 \varphi$ and $Y = \dot{X}$, one has the parameterization by the algebraic complex curve

$$\begin{aligned} Y^2 &= 4(1-X)[(2h + 2p_r \delta + 2p_r \gamma) + (\delta^2 - p_\theta^2 - 2h - 4p_r \delta - 2p_r \gamma)(1-X) \\ &+ (-2\delta^2 + 2p_r \delta)(1-X)^2 + \delta^2(1-X)^3]. \end{aligned}$$

As the degree in the right-hand side is less or equal to four, the genus is at most one so φ is rational or elliptic. Using the bi-rational transform $u = 1/(1-X)$ to send the fix root $X = 1$ (that is $\varphi = \pi/2$, equator) to infinity,

$$(Yu^2)^2 = 4[\xi^2 u^3 + (\delta^2 - p_\theta^2 - 2\delta p_r - \xi^2)u^2 + (-2\delta^2 + 2\delta p_r)u + \delta^2] \quad (4)$$

with $\xi^2 = 2h + 2(\delta + \gamma)p_r$. Obviously,

Lemma 2.1. *The points $(0, \delta^2)$ and $(1, -p_\theta^2)$ belong to the elliptic curve (4).*

Proposition 3. *Assume $\delta > 0$ and $p_\theta \neq 0$.*

- (i) *When $\xi = 0$, the (complex) curve is rational.*
- (ii-a) *When $\xi^2 > 0$, the curve is elliptic and parameterized by the unbounded component of the elliptic curve.*
- (ii-b) *When $\xi^2 < 0$, the curve is elliptic and parameterized by the bounded component of the imaginary elliptic curve.*

Proof. Inspecting the graph of the cubic in (4) right-hand side, it is clear using the previous lemma that for $\xi^2 > 0$ (resp. < 0) the unbounded component of the real elliptic curve alone (resp. the bounded component of the imaginary elliptic curve) is admissible since $u \geq 1$ ($u = 1/(1-X)$ with $X = \sin^2 \varphi$). \square

Disregarding the simpler rational situation, we assume $\xi \neq 0$ and use affine coordinates for the homogeneous parameter $[\xi : p_r : p_\theta : \delta : \gamma]$ to get

$$w^2 = 4[u^3 + (\bar{\delta}^2 - \bar{p}_\theta^2 - 2\bar{\delta}\bar{p}_r - 1)u^2 + (-2\bar{\delta}^2 + 2\bar{\delta}\bar{p}_r)u + \bar{\delta}^2] \quad (5)$$

where $w = Yu^2/\xi$, $\bar{p}_r = p_r/\xi$, etc. In Weierstraß form, we finally have $w^2 = 4v^3 - g_2v - g_3$ with

$$u = v - a, \quad a = \frac{1}{3}(\bar{\delta}^2 - \bar{p}_\theta^2 - 2\bar{\delta}\bar{p}_r - 1), \quad (6)$$

and invariants g_2, g_3 rational in the parameters.¹

Proposition 4. *Trajectories of the normal flow in the integrable case are the following,*

$$\begin{aligned} \sin^2 \varphi &= 1 - \frac{1}{\wp(\xi t + z_0) - a}, \quad \wp(z_0) = a + \frac{1}{\cos^2 \varphi_0}, \\ \theta &= \theta_0 + \frac{p_\theta}{\wp'(z_1)} \left[2\zeta(z_1)t + \frac{1}{\xi} \ln \frac{\sigma(\xi t + z_0 - z_1)}{\sigma(\xi t + z_0 + z_1)} \right]_0^t, \quad z_1 \text{ s.t. } \wp(z_1) = a + 1, \\ r &= r_0 - (\delta + \gamma)t \\ &\quad + \frac{\delta}{\wp'(z_2)} \left[2\zeta(z_2)t + \frac{1}{\xi} \ln \frac{\sigma(\xi t + z_0 - z_2)}{\sigma(\xi t + z_0 + z_2)} \right]_0^t, \quad z_2 \text{ s.t. } \wp(z_2) = a, \end{aligned}$$

with Weierstraß invariants and a defined according to (5-6). Let $2\omega\mathbf{Z} + 2\omega'\mathbf{Z}$ denote the real rectangular lattice of periods, and τ (resp. T) denote the period of $X = \sin^2 \varphi$ (resp. of φ).

(i) When $\xi^2 > 0$, $\tau = 2\omega/\xi$ and $T = 2\tau$ (tall extremals).

(ii) When $\xi^2 < 0$, $\tau = 2\omega'/\xi$ and $T = \tau$ (small extremals).

Proof. Introducing Weierstraß functions ζ and σ , $\zeta' = -\wp$, $\sigma'/\sigma = \zeta$, one has

$$\int \frac{\wp'(z_0)dz}{\wp(z) - \wp(z_0)} = 2\zeta(z_0)z + \ln \frac{\sigma(z - z_0)}{\sigma(z + z_0)},$$

whence the quadratures on r and θ . The time law is $dt = dz/\xi$, so one has $\tau = 2\omega/\xi$ when $\xi^2 > 0$ since $z \in [0, 2\omega]$ is the uniform parameterization of the unbounded component of the real elliptic curve. Conversely, $\tau = 2\omega'/\xi$ when $\xi^2 < 0$ since $z \in \omega + [0, 2\omega']$ is the parameterization of the bounded component of the imaginary elliptic curve. As $X = 1 - 1/(\wp - a)$, $X = 1$ is reached if and only if $\wp = \infty$, that is only on the unbounded component. In this case, since $[0, \pi] \ni \varphi \rightarrow \sin^2 \varphi$ covers twice $[0, 1]$, φ crosses the equator $\varphi = \pi/2$ and is extended beyond by symmetry ($\varphi \mapsto \pi - \varphi$, tall extremal). It remains otherwise on the same hemisphere— $(0, \pi/2)$ or $(\pi/2, \pi)$, depending on the initial condition—, thus defining a *small* extremal. \square

3. Conjugate and cut loci. We recall the following standard notions of Riemannian geometry [1] and optimal control. A *cut point* is the first point (if any) along an extremal such that the extremal ceases to be minimizing. Given an initial condition x_0 , the *cut locus* is the set of such points on extremals departing from x_0 . A

¹That the invariants depend rationally on parameters is useful for further computations on the quadratures (e.g., cut or conjugate point evaluation). See [2, 3, 8] for such analyses.

point $x(t_c)$ on an extremal $z = (x, p)$ is conjugate to x_0 if there exists a *Jacobi field* $\delta z = (\delta x, \delta p)$, solution of the linearized system along the extremal,

$$\delta \dot{z} = d\vec{H}(z(t))\delta z, \quad \vec{H} = (\partial_p H, -\partial_x H),$$

which is non-trivial ($\delta x \not\equiv 0$) and vertical at $t = 0$ and t_c , $\delta x(0) = \delta x(t_c) = 0$. The *conjugate locus* is the set of such first points on extremals departing from x_0 . Conjugacy is classically related to local optimality of extremals in the relevant topologies.

We focus on the restriction to $p_r = 0$ of the integrable case. According to Proposition 2, the resulting Hamiltonian

$$H = \frac{1}{2} \frac{p_\theta^2}{\tan^2 \varphi} + \frac{1}{2} (p_\varphi - \delta \cos \varphi \sin \varphi)^2 - \frac{1}{2} \delta^2 \cos^2 \varphi \sin^2 \varphi \quad (7)$$

defines a three-dimensional Lorentzian metric with a singularity at $\varphi = \pi/2$, and describes the control system when the r -coordinate is not taken into account. The metric is actually Riemannian on \mathbf{S}^2 when $\delta = 0$ (with the same equatorial singularity) and has been studied in [2, 4], so that (7) can also be interpreted as a Zermelo-like deformation (presence of a drift) of this Riemannian situation when $\delta > 0$.

Theorem 3.1. (See Figs. 1-2.) Let $p_r = \delta = 0$. (i) When $\varphi_0 \neq \pi/2$, the cut locus is a single antipodal branch and the conjugate locus is astroidal with two horizontal and two vertical cusps. (ii) When $\varphi_0 = \pi/2$, the cut locus is the equator minus the initial point and the conjugate locus is double-heart shaped with four vertical cusps.

For $\delta > 0$, we exclude the singular case $\varphi_0 = \pi/2$ and provide some preparatory numerical insight into the structure of cut and conjugate loci. The following is clear (see Fig. 3).

Proposition 5. Pairs of extremals of the normal integrable submodel defined by $\pm \dot{\varphi}(0)$ intersect at $t = \tau$ with same cost. Intersections are antipodal on $\varphi = \pi - \varphi_0$ for tall extremals, on $\varphi = \varphi_0$ for small ones.

Beside intersections of small extremals, another new phenomenon compared to the Riemannian case ($\delta = 0$) is the existence of extremals intersecting with same cost (and time) belonging to different Hamiltonian level sets, as illustrated by Fig. 4.

In the Riemannian situation, one can restrict to the level $H = 1/2$ and parameterize so geodesics by arc length. Equivalently, one may fix the final time and obtain geodesics by varying the level set. In the Lorentzian case, the second approach still makes sense. We normalize the final time to $t_f = 1$ and consider the h -curves generated by varying the level set. More precisely, restricting to $p_r = 0$ and having fixed $\delta > 0$ and $\varphi_0 \neq \pi/2$, we parameterize $T_{(0, \varphi_0)}^* \mathbf{S}^2$ (θ_0 is set to zero) according to

$$\frac{p_{\theta_0}}{\tan \varphi_0} + i(p_{\varphi_0} - \delta \cos \varphi_0 \sin \varphi_0) = \rho e^{i\alpha}, \quad 2h + \delta^2 \cos^2 \varphi_0 \sin^2 \varphi_0 = \rho^2. \quad (8)$$

To any direction α of initial adjoint vector is associated an h -curve,

$$h \mapsto \exp_{\varphi_0, \delta}(h, \alpha)$$

where the exponential is the projection on the (θ, φ) -space of the integral curve of H with initial condition $(0, \varphi_0, p_{\theta_0}, p_{\varphi_0})$, the initial adjoints being defined by (h, α) in accordance with (8). These h -curves are evaluated numerically, and conjugate points occurring at t_f are computed by [9] along them. We are thus able to obtain the section at $t = t_f$ of the conjugate locus, as well as the isocost lines or *wavefront*.

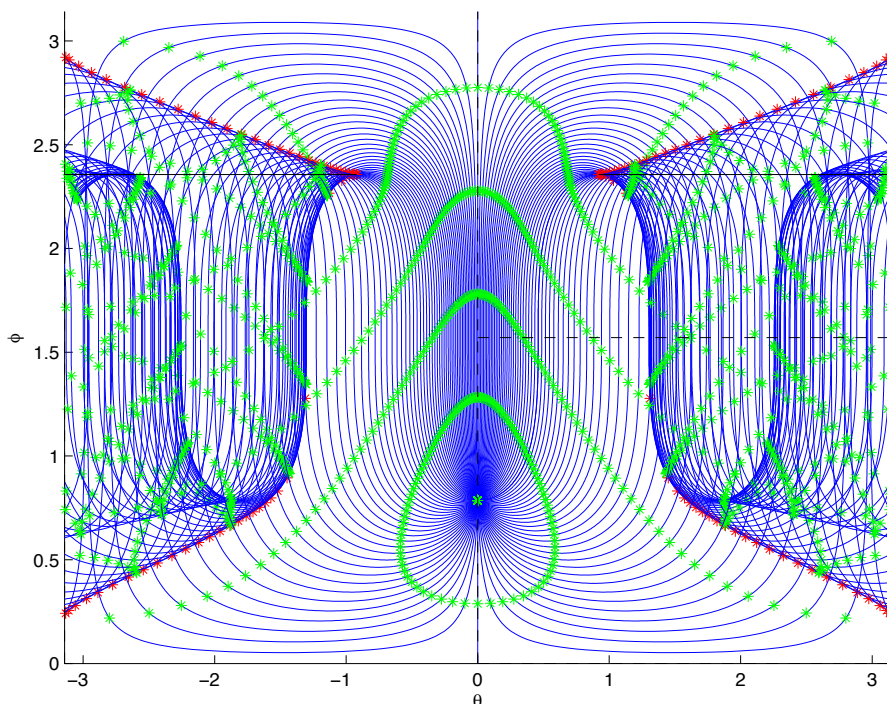


FIGURE 1. Cut and conjugate loci, $p_r = 0$, $\delta = 0$, $\varphi_0 = \pi/4$. Geodesics in blue, isocost lines green, cut locus black, conjugate locus red. The cut locus is a closed single branch (the two halves towards $\theta = \pm\pi$ are portrayed in the covering) included in the antipodal parallel, $\varphi = \pi - \varphi_0$. The conjugate locus has two horizontal and two vertical cusps (astroid-like locus on the sphere).

The results displayed Figs. 5-9 provide a first insight into the structure of cut and conjugate loci for positive δ . In particular, antipodal cut points labeled I.a analogous to those of the Riemannian case are preserved. The same symmetry on small extremals generate cut points I.b, provided δ is big enough.² (Compare $\delta = 4$ and $\delta = 5.6$ in the aforementioned figures.) The results for larger values of δ indicate a more intricate structure of both cut and conjugate loci (see Figs. 8-9) that will be the subject of future investigation.

Acknowledgments. We thank Mohamed Biari for his help with preliminary numerical computations.

REFERENCES

- [1] M. Berger, *A panoramic view of Riemannian geometry*, Springer, 2003.
- [2] B. Bonnard and J.-B. Caillau, *Singular metrics on the two-sphere in space mechanics*, preprint (2008), hal.archives-ouvertes.fr/hal-00319299.
- [3] B. Bonnard, J.-B. Caillau, and L. Rifford, *Convexity of injectivity domains on the ellipsoid of revolution: The oblate case*, C. R. Acad. Sci. Paris, Sér. I **348** (2010), 1315–1318.

²The six-cusp structure of the conjugate locus displayed in the covering of the two-sphere minus the poles is a reminder of the *laughing curve* in [11], though singularities appear at different places.

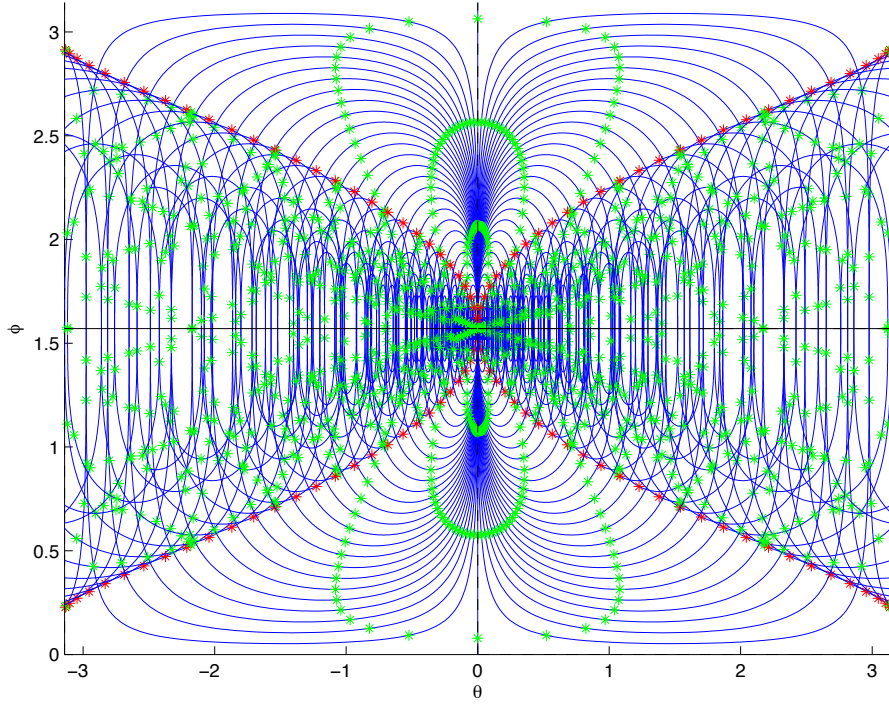


FIGURE 2. Cut and conjugate loci, $p_r = 0$, $\delta = 0$, $\varphi_0 = \pi/2$. Geodesics in blue, isocost lines green, cut locus black, conjugate locus red. For the initial condition at singularity, the cut locus is the whole equator minus the starting point. The conjugate locus has four vertical cusps (double-heart shaped locus on the sphere, see [4]).

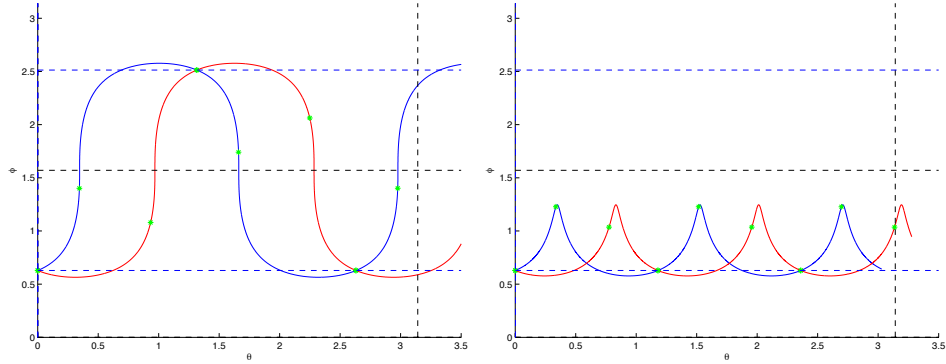


FIGURE 3. Intersecting extremals, $\pm\dot{\varphi}(0)$ symmetry. Pair of tall extremals ($\xi^2 > 0$) on the left, small extremals ($\xi^2 < 0$) on the right, both intersecting with same cost for t_f equal to the period of $X = \sin^2 \varphi$ (tall ones are obtained by symmetrically unfolding small ones reaching $\varphi = \pi/2$). In both cases, intersecting extremals belong to the same Hamiltonian level. These intersections generate cut points I.a (tall ones) and I.b (small ones), see Figs. 5-9. These points belong respectively to the antipodal line $\varphi = \pi - \varphi_0$ and to $\varphi = \varphi_0$.

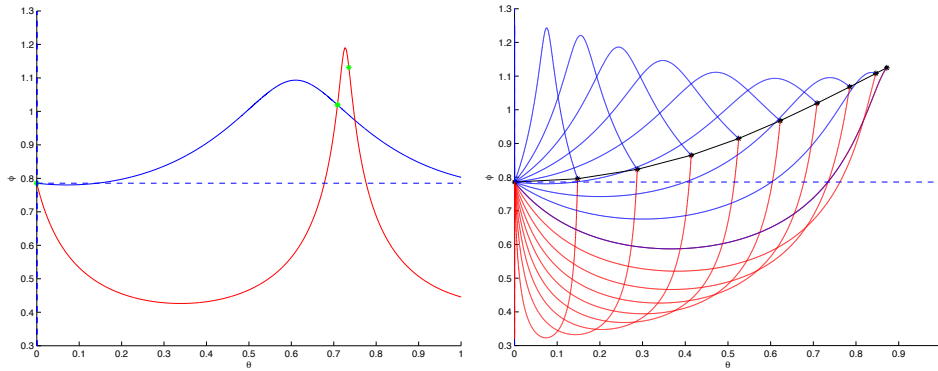


FIGURE 4. Small extremals on different Hamiltonian level sets intersecting with same cost, $p_r = 0$, $\delta = 4$, $\varphi_0 = \pi/4$. Left, the first intersection point occurs at $t_f = 1$ on $h \simeq -1.095$ (blue) and $h \simeq -9.486e - 1$ (red), respectively. Right, a whole family of such pairs of extremals intersecting at $t_f = 1$ with same cost is portrayed. These intersection points generate part II of the cut locus, see Figs. 5-9.

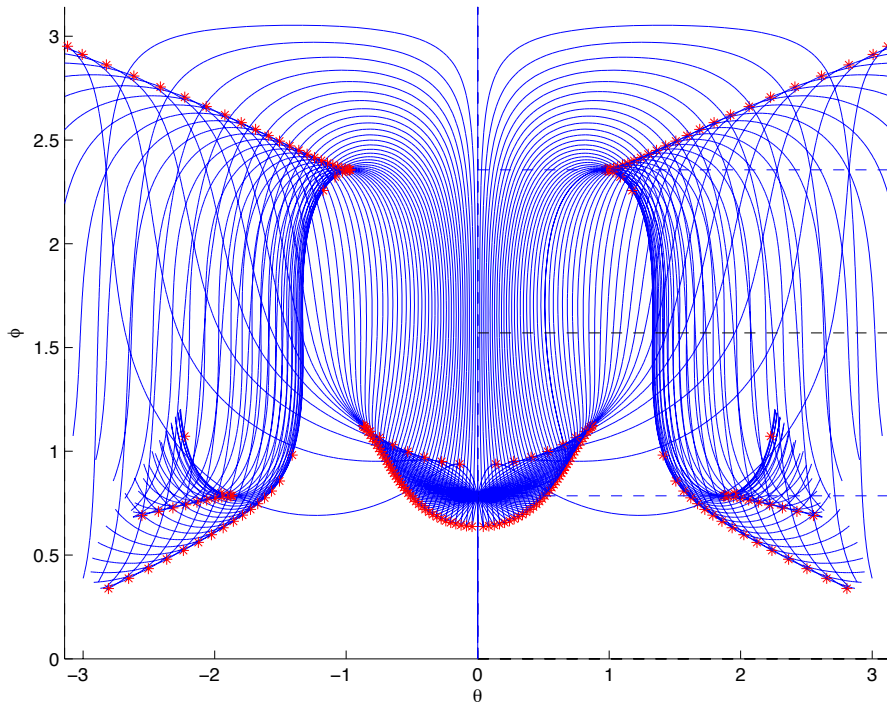


FIGURE 5. H-curves and conjugate locus, $p_r = 0$, $\delta = 4$, $\varphi_0 = \pi/4$. The conjugate locus (red) is the envelope of h-curves (blue). The four cusps (two horizontal and two vertical) of the conjugate locus are preserved (astroidal part compare Fig. 1, $\delta = 0$) while a new smile-shaped component with two cuspidal singularities of the locus appears. Small parts of the second conjugate locus are also portrayed.

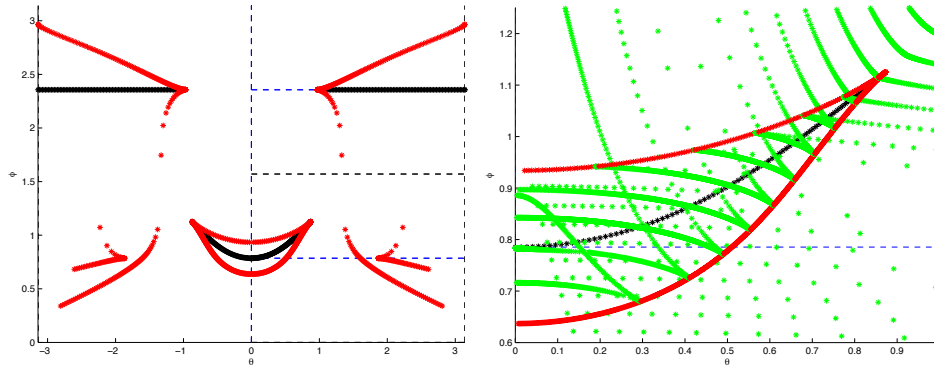


FIGURE 6. Cut and conjugate loci, wavefront, $p_r = 0$, $\delta = 4$, $\varphi_0 = \pi/4$. Left, the antipodal part I.a of the cut locus (black) is preserved (compare Fig. 1, $\delta = 0$). The new component II with extremities located at the singularities of the smile-shaped part of the conjugate locus appears. Right, isocost lines (green) defining the wavefront are portrayed. Self-intersections of the front define cut points II (black) while its swallowtail singularities run along the conjugate locus (red) obtained as a caustic.

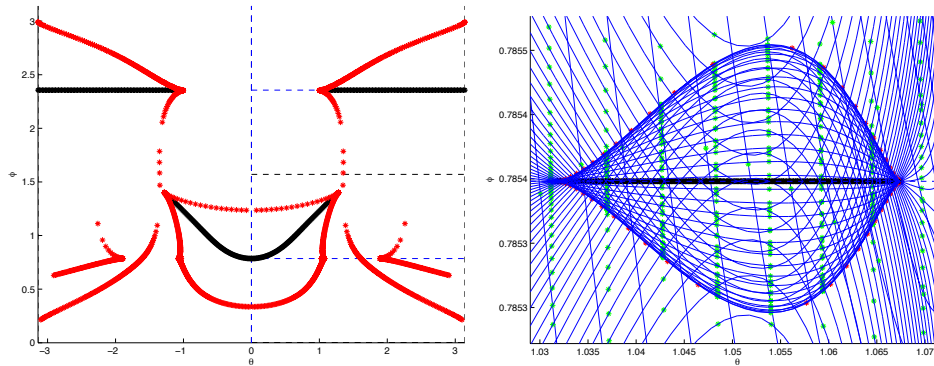


FIGURE 7. Cut and conjugate loci, h-curves, $p_r = 0$, $\delta = 5.6$, $\varphi_0 = \pi/4$. Left, the astroidal and smile-shaped parts of the conjugate locus are preserved (compare Fig. 6, $\delta = 4$). Two new components (symmetry wrt. $\theta = 0$) of the conjugate locus appear (detail on the rightmost picture), slightly deforming the smiling-shaped part in their neighbourhood. Right, detail of h-curves (blue) generating a new component (the right one, $\theta \geq 0$) of the conjugate locus (red) with two horizontal cusps. The corresponding right new component of the cut locus (black) appearing has its extremities located at these singularities. It is a single branch included in the parallel $\varphi = \varphi_0$ formed by cut points I.b (intersections of symmetric small extremals, see Fig. 3). The same is observed on $\theta \leq 0$.

[4] B. Bonnard, J.-B. Caillaud, R. Sinclair and M. Tanaka, *Conjugate and cut loci of a two-sphere of revolution with application to optimal control*, Ann. Inst. H. Poincaré Anal. Non Linéaire **26** (2009), no. 4, 1081–1098.

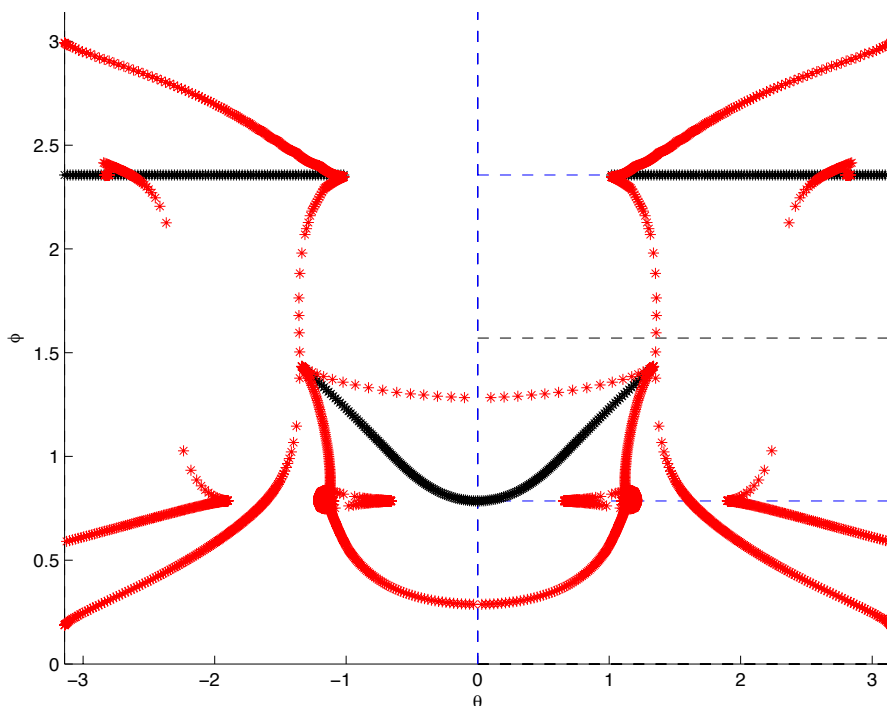


FIGURE 8. Cut and conjugate loci, $p_r = 0$, $\delta = 6$, $\varphi_0 = \pi/4$. The astroidal part of the conjugate locus (red) is preserved while new singularities and self-intersections appear on the smile-shaped part (detail on Fig. 9). One of the cusps of each of the two new components observed Fig. 7 disappears. Parts I.a and II of the cut locus (black) are preserved.

- [5] B. Bonnard, M. Chyba and D. Sugny, *Time-minimal control of dissipative two-Level quantum systems: The generic case*, IEEE Trans. Autom. Control **54** (2009), no. 11, 2598–2610.
- [6] B. Bonnard, O. Cots, N. Shcherbakova and D. Sugny, *The energy minimization problem for two-level dissipative quantum systems*, J. Math. Phys. **51** (2010), 092705.
- [7] U. Boscain, G. Charlot, J.-P. Gauthier, S. Guérin and H.-R. Jauslin, *Optimal control in laser-induced population transfer for two- and three-level quantum systems*, J. Math. Phys. **43** (2002), no. 5, 2107–2132.
- [8] J.-B. Caillau, B. Daoud and J. Gergaud, *On some Riemannian aspects of two and three-body controlled problems*, in “Recent Advances in Optimization and its Applications in Engineering”, 205–224, Springer, 2010.
- [9] J.-B. Caillau, O. Cots and J. Gergaud, *Differential continuation for regular optimal control problems*, Optim. Methods Softw., to appear, apo.enseeiht.fr/hamopath.
- [10] N. Khaneja, S. J. Glaser and R. Brockett, *Sub-Riemannian geometry and time optimal control of three spin systems: Quantum gates and coherence transfer*, Phys. Rev. A **65** (2002), no. 3, 11 p.
- [11] B. Mazur, *Perturbations, deformations, and variations (and “near-misses”) in geometry, physics, and number theory*, Bull. American Math. Soc. **41** (2004), no. 3, 307–336.

Received August 2010; revised March 2011.

E-mail address: bernard.bonnard@u-bourgogne.fr

E-mail address: jean-baptiste.caillau@u-bourgogne.fr

E-mail address: olivier.cots@u-bourgogne.fr

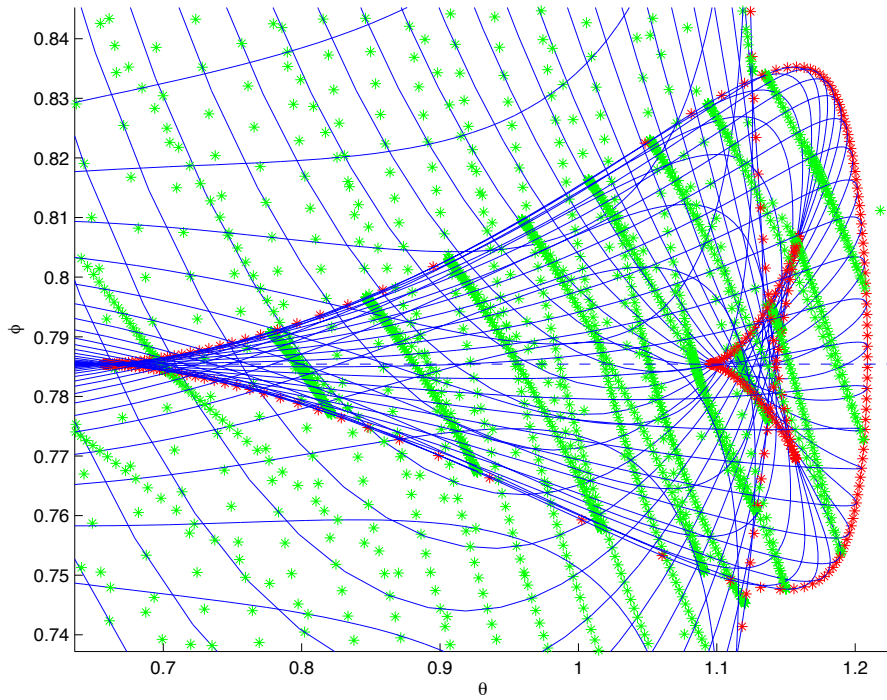


FIGURE 9. H-curves, conjugate locus and wavefront, $p_r = 0$, $\delta = 6$, $\varphi_0 = \pi/4$ (detail). The smile-shaped part of the conjugate locus (red) now self-intersects and has three additional cusps on its right part (the same is observed for $\theta \leq 0$), suggesting a more complicated structure of the cut locus in its neighbourhood. The right new component of the conjugate locus observed for $\delta = 5.6$ now just has one cusp. The swallowtail singularities of the wavefront (green) suggest that part of the cut points of type I.b persist on $\varphi = \varphi_0$.